MNRAS **000**, 1–?? (2024) Preprint 12 April 2025 Compiled using MNRAS LATEX style file v3.0

Long-term evolution of BH-ULX candidates: An 'unusual' $L_{\rm disc} - T_{\rm col}$ correlation associated with spectral states

Seshadri Majumder[1]⋆, Santabrata Das[1]† and Anuj Nandi[2]‡
[1]*Department of Physics, Indian Institute of Technology Guwahati, Guwahati, 781039, India.*
[2]*Space Astronomy Group, ISITE Campus, U. R. Rao Satellite Centre, Outer Ring Road, Marathahalli, Bangalore, 560037, India.*

Accepted XXX. Received YYY; in original form ZZZ

ABSTRACT

We present the long-term spectral evolution of eight black hole ultra-luminous X-ray sources (BH-ULXs), namely NGC1313 X−1, NGC5408 X−1, NGC6946 X−1, IC342 X−1, NGC55 ULX1, NGC4395 ULX1, NGC5204 X−1 and NGC4190 ULX1 using *XMM-Newton* monitoring data spanning over a decade or more. An in-depth spectral modeling with thermal Comptonization (`nthComp`) and standard disc (`diskbb`) components reveals NGC5204 X−1, IC342 X−1, NGC4190 ULX1 and NGC1313 X−1 exhibiting harder spectral characteristics with dominant effect of Comptonization ($F_{\rm nth} > F_{\rm disc}$, $\Gamma_{\rm nth} \lesssim 2$). However, NGC6946 X−1 and NGC55 ULX1 remain in a disc-dominated state ($F_{\rm disc} \sim 2F_{\rm nth}$, $\Gamma_{\rm nth} \gtrsim 2$), while NGC5408 X−1 shows intermediate spectral characteristics. The spectral analyses indicate an anti-correlation between disc luminosity ($L_{\rm disc}$) and temperature ($T_{\rm col}$) for all sources except NGC5204 X−1. These anti-correlations follow a relation $L_{\rm disc} \propto T_{\rm col}^{\alpha}$ with steeper exponents of $\alpha = -6.01 \pm 0.25$ (NGC55 ULX1), -8.93 ± 0.11 (NGC6946 X−1), and -10.31 ± 0.10 (NGC5408 X−1) for sources with softer or intermediate spectral characteristics. For harder sources, NGC1313 X−1 and IC342 X−1, the combined results provide $\alpha = -3.58 \pm 0.04$. However, for NGC5204 X−1, a positive correlation is found, yielding $\alpha = 1.4 \pm 0.1$, suggesting that the emission mechanism is associated with the transition from the 'standard disc' to the 'slim disc' scenario. These findings suggest that the observed $L_{\rm disc} - T_{\rm col}$ correlations, along with the overall spectro-temporal properties of BH-ULXs, seems to be governed by disc-corona-wind driven accretion processes at various inclinations. Finally, we report a QPO-like feature ($\sim$ 20 mHz) with $rms\% \sim 6.6$, Q-factor ~ 6.7 and significant 2.8σ in NGC55 ULX1.

Key words: accretion, accretion disc – black hole physics – X-rays: galaxies – radiation mechanisms: general – stars: individual

1 INTRODUCTION

Ultraluminous X-ray sources (ULXs) are the class of extragalactic, point-like, non-nuclear objects with isotropic luminosity in excess of 10^{39} erg s^{-1} (Fabbiano 1989; Makishima et al. 2000a). Despite being discovered more than thirty years ago, the exact nature of these objects remains a point of debate and their observational features are still not well understood (see Feng & Soria 2011; Kaaret et al. 2017; Fabrika et al. 2021; King et al. 2023, for a recent review). Based on the observational evidences from timing and spectral variability, a population of the ULXs are believed to be powered by super-Eddington accretion onto stellar-mass black holes (Bachetti et al. 2013; Walton et al. 2013, 2014, 2015; Rana et al. 2015, see references therein). The presence of massive stellar-mass black holes in several ULXs is also suggested (Agrawal & Nandi 2015; Das et al. 2021; Majumder et al. 2023). Alternatively, a plausible scenario relying on the intermediate-mass black holes (IMBHs) of mass $\gtrsim 100 M_{\odot}$ as the powerhouse of such extremely luminous systems is also propounded (Colbert & Mushotzky 1999; Makishima et al. 2000b; Miller et al. 2003; Das et al. 2021; Majumder et al. 2023). In addition, the possibility of having highly magnetized neutron stars at the central core is also put forward to explain the pulsations detected in several ULXs (Bachetti et al. 2014; Fürst et al. 2016; Israel et al. 2017; Carpano et al. 2018; Sathyaprakash et al. 2019; Rodríguez Castillo et al. 2020; Quintin et al. 2021).

⋆ E-mail: smajumder@iitg.ac.in
† E-mail: sbdas@iitg.ac.in
‡ E-mail: anuj@ursc.gov.in

The temporal variability of ULXs has been studied in several sources over the past few decades. However, interpretation of the physical origin of these variability properties remains challenging. For example, based on the observed variability in the power density spectra, Heil et al. (2009) proposed that a sample of bright ULXs of comparable luminosity can be divided into two groups − one showing very weak variability on the timescale of about 100 s, whereas another exhibiting similar variability properties, observed in most of the black hole X-ray binaries (BH-XRBs) (Belloni et al. 2005; Nandi et al. 2012; Athulya et al. 2022; Aneesha et al. 2024). Intriguingly, the mechanism that suppresses the intrinsic variability in one group of ULXs remains under debate (Heil et al. 2009; Feng & Soria 2011). Interestingly, the fractional variability amplitude ($f_{\rm var}$), indicative of the amount of variability, is found to be low ($\lesssim$ 10%) in the hard-ultraluminous states (HUL) as compared to the soft-ultraluminous states (SUL) with $f_{\rm var} \sim 10 - 30\%$ (Sutton et al. 2013). Further, several ULXs are also reported to exhibit Quasi-periodic Oscillations (QPOs) in the presence of flat-topped noise in the power density spectra (Dewangan et al. 2006; Strohmayer et al. 2007; Feng et al. 2010; Rao et al. 2010; Pasham et al. 2015; Agrawal & Nandi 2015; Atapin et al. 2019; Majumder et al. 2023). In addition, it has been proposed that the observed QPOs are possibly generated due to the modulation of the Comptonizing corona, present at the inner accretion flow and that serves as a powerful tool to probe the accretion scenarios of the ULXs harboring black hole accretors (Das et al. 2021; Majumder et al. 2023).

Needless to mention that the spectral morphologies of ULXs are well studied in X-rays with dedicated missions like *XMM-Newton*, *Chandra* and *NuSTAR* over the years. Interestingly, the ULX spectra up to $\sim$ 10 keV can be classified into two distinct types: one described by simple power-law and the other exhibiting a broad spectral curvature over the entire energy band (Feng & Soria 2011). Generally, a high power-law photon index of $\Gamma \gtrsim 3$ is seen for the sources of softer characteristics, whereas $\Gamma \sim 1$ is observed in a few harder sources. Notably, some of the hard power-law dominated ULXs show significant flux variability (Feng & Kaaret 2009; Kaaret & Feng 2009; Soria & Ghosh 2009) similar to the hard state of BH-XRBs (Belloni et al. 2005; Remillard & McClintock 2006). Thus, the interpretation of power-law dominated spectral state in ULXs as the canonical hard state of BH-XRBs would imply a black hole of mass $\gtrsim 10^3\ M_\odot$ (Winter et al. 2006; Feng & Soria 2011). Meanwhile, a good number of high-quality observations from XMM-Newton could detect the soft excess in low energies ($<$ 2 keV) and curvature around $\sim 3 - 10$ keV in ULX spectra (Ghosh & Rana 2021, and references therein) unlike the BH-XRBs, showing a spectral turnover at relatively higher energies (Xu et al. 2019). Further, it has been suggested that the high energy curvature could arise from the innermost hot accretion flow as a result of the interception of disc photons into the Comptonizing corona (Middleton et al. 2015; Mukherjee et al. 2015; Jithesh 2022). In contrast, the soft excess below $\sim$ 2 keV is thought to be originated from the outflowing wind or entirely from the disc emission alone (Poutanen et al. 2007; Middleton et al. 2015).

The extensive monitoring with *XMM-Newton*, *Chandra*, *NuSTAR* and *Swift-XRT* enables the opportunity of studying the long-term spectro-temporal evolution of ULXs. So far, a handful of sources have been studied in quest of the long-term variation of ULX characteristics. For example, Gúrpide et al. (2021) reported the spectral evolution for a group of ULXs, revealing the origin of variability in these systems. In addition, the transition between several spectral states is conjectured from the long-term monitoring of a number of ULXs (Yoshida et al. 2010). Further, the long-term monitoring of NGC 5408 X−1 with *Swift-XRT* reveals dipping behavior in the light curve, possibly connected to the super-orbital phenomenon, similar to some of the BH-XRBs (Grisé et al. 2013).

In this work, we consider eight BH-ULXs, namely NGC 1313 X−1, NGC 5408 X−1, NGC 6946 X−1, IC 342 X−1, NGC 55 ULX1, NGC 4395 ULX1, NGC 5204 X−1 and NGC 4190 ULX1, having decade-long observations with *XMM-Newton*. The sources are primarily selected based on the publicly available *XMM-Newton* observations spanning over about a decade and the previous predictions of having black hole accretors at the central core of these objects. Out of this eight sources, a detailed spectro-temporal study is carried out for five sources (NGC 1313 X−1, NGC 5408 X−1, NGC 6946 X−1, M 82 X−1 and IC 342 X−1) that show mHz QPO features (Majumder et al. 2023, hereafter Paper-I). Note that, the BH-ULX candidate NGC 247 ULX1 was not studied in Paper-I due to the absence of any reported QPO detections for this source. It is worth mentioning that M82 X−1 is kept aside from the present work irrespective of having multiple observations because of the significant contamination from nearby objects in the *XMM-Newton* aperture (see Majumder et al. 2023 and references therein). Moreover, a preliminary analysis of the variability properties of NGC 247 ULX1 suggests that the source exhibits a dipping behavior in its light curves (see Alston et al. 2021 also), accompanied by supersoft characteristics, which remain distinct from that of other sources. Therefore, we exclude NGC 247 ULX1 in this study. Note that, the four sources, namely NGC 55 ULX1, NGC 4395 ULX1, NGC 5204 X−1 and NGC 4190 ULX1, have been relatively less studied and serve as ideal targets for detailed analysis. With the exception of the above source selection criteria, NGC 4190 ULX1—often referred to as the 'forgotten ULX' due to its intriguing yet relatively unexplored characteristics—is also considered in this work, despite having only three observations with *XMM-Newton*. Below, we present the brief characteristics of the four sources for which an in-depth analysis has been performed in this work.

- NGC 55 ULX1 is the brightest ULX in the spiral galaxy NGC 55 at a distance of 1.94 Mpc[1] with a peak luminosity of $\sim 4 \times 10^{39}$ erg s^{-1}. Interestingly, in most of the previous studies, the source was found in the SUL state with disc-dominated spectra (Jithesh 2022; Barra et al. 2022).
- NGC 4395 ULX1 is one of the ULXs located in the NGC 4395 galaxy at a distance of 4.76 Mpc with luminosity $\sim 3 \times 10^{39}$ erg s^{-1} (Ghosh et al. 2022). Detailed spectral study with *XMM-Newton* and *Chandra* observations rules out the possibility of having an SUL state by confirming its steep power-law tail (Earnshaw & Roberts 2017).

[1] https://ned.ipac.caltech.edu

- The source NGC 5204 X−1 is located ∼ 15 arcsec away from the centre of the host galaxy NGC 5204 at a distance of 4.8 Mpc. The evidence of significant outflows resulting in several emission features is observed in NGC 5204 X−1 with *XMM-Newton* (Kosec et al. 2018).
- The low surface brightness galaxy NGC 4190 located at a distance of 3 Mpc contains NGC 4190 ULX1, a bright ULXs of luminosity $\sim (3-10)\times10^{39}$ erg s^{-1} (Ghosh & Rana 2021). The mass of the source is predicted to be in the range of $10-30M_{\odot}$, indicating the presence of a stellar-mass black hole in the system (Ghosh & Rana 2021). Recently, a super-Eddington slim disc scenario is also suggested for NGC 4190 ULX1 (Earnshaw et al. 2024).

In this work, we carry out a detailed long-term spectro-temporal analysis of the selected BH-ULXs using the archival *XMM-Newton* observations spanning over a decade. Towards this, we investigate the spectral characteristics of the sources by modeling the *XMM-Newton* spectra in 0.3−10 keV energy range with the combination of physically motivated models, describing different emission mechanisms. Investigation of the spectral properties indicates the presence of both positive and negative correlations between the bolometric disc luminosity ($L_{\rm disc}$) and the disc temperature. The correlation properties are observed to be closely connected with the distinct spectral states, obtained from the long-term evolution of the sources. Finally, we find that the disc-corona-wind regulated accretion scenario described by the Keplerian and sub-Keplerian flow components is capable in explaining the spectro-temporal findings of the BH-ULXs.

The paper is organized as follows. In §2, we briefly mention the *XMM-Newton* observations of the sources and the standard data reduction procedure of *EPIC-PN* and *EPIC-MOS* instruments. The results of spectral and timing analyses are presented in §3. In §4, we infer the possible physical scenarios to delineate the findings and summarize the results in §5.

2 OBSERVATION AND DATA REDUCTION

We look into the `HEASARC` public data archive[2] for all the observations of NGC 55 ULX1, NGC 4395 ULX1, NGC 5204 X−1 and NGC 4190 ULX1 with *XMM-Newton*. We find that the sources are observed on several occasions by *XMM-Newton* and except NGC 4190 ULX1, all the sources have at least ten or twenty years of monitoring. In Table 1, we tabulate the details of all the observations considered in this work. We find a total of thirty-one observations considering all the sources. However, we note that several observations suffer from various caveats (see Remarks on Table 1) and hence are excluded from the analysis.

The *XMM-Newton* data extraction of the remaining observations is carried out following the analysis threads[3] provided by the instrument team. The data reduction software `SCIENCE ANALYSIS SYSTEM (SAS) V21.0.0`[4] is used to analyze the data. We run the tasks `epproc` and `emproc` to generate the event files for *EPIC-PN* and *EPIC-MOS* instruments, respectively. The high energy particle background flares are identified and clean event files are filtered out following Majumder et al. (2023). We adopt the event selection criteria as `PATTERN` ≤ 4 and `PATTERN` ≤ 12 with `FLAG`= 0 while generating the scientific products from *EPIC-PN* and *EPIC-MOS* data, respectively. Following the previous studies, we select the source regions while extracting the light curves and spectra as 40 arcsec, 25 arcsec, 30 arcsec and 40 arcsec for NGC 55 ULX1 (Jithesh 2022), NGC 4395 ULX1 (Ghosh et al. 2022), NGC 4190 ULX1 (Ghosh & Rana 2021) and NGC 5204 X−1 (Gúrpide et al. 2021), respectively. Further, we select the same circular radii for the respective sources in a source-free area on the same *EPIC* chip to generate the background light curves and spectra. For spectral analysis, each spectrum is grouped with 25 counts per spectral channel using the `specgroup`[5] tool of `SAS`.

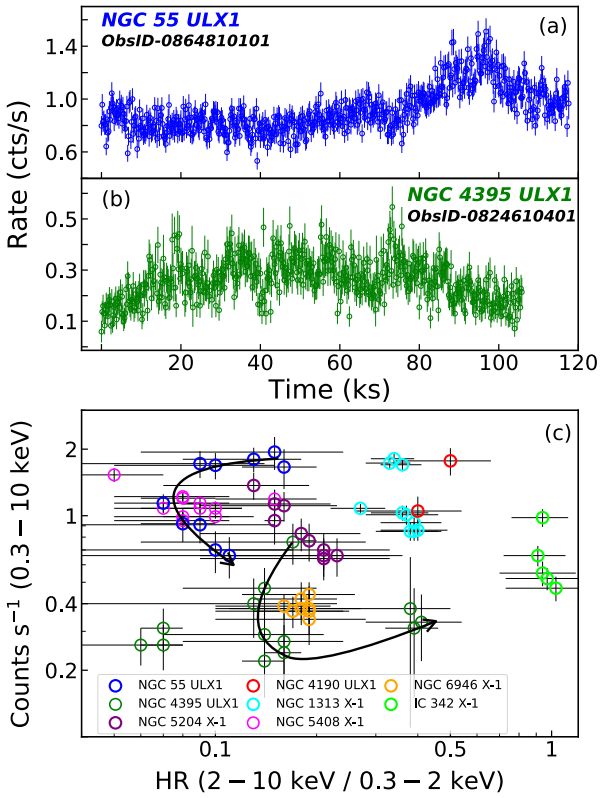

Figure 1. Panel (a)-(b): Background subtracted 200 s binned *EPIC-PN* light curves of NGC 55 ULX1 and NGC 4395 ULX1 in 0.3 − 10 keV energy range. Panel (c): Hardness-intensity diagram (HID) of all eight BH-ULXs considered in this work. The open circles of different colors denote the HID of the respective sources. The results for NGC 6946 X−1, NGC 1313 X−1, IC 342 X−1 and NGC 5408 X−1 are adopted from Paper-I (Majumder et al. 2023). In panel (c), the black curved arrows represent the 'C-shaped' patterns observed in the HID of NGC 55 ULX1 and NGC 4395 ULX1, respectively. See the text for details.

[2] https://heasarc.gsfc.nasa.gov/db-perl/W3Browse/w3browse.pl
[3] https://www.cosmos.esa.int/web/xmm-newton/sas-threads
[4] https://www.cosmos.esa.int/web/xmm-newton/sas
[5] https://xmm-tools.cosmos.esa.int/external/sas/current/doc/specgroup/index.html

Table 1. Details of the *XMM-Newton* observations analyzed in this work of the four selected BH-ULXs. In the table, all the symbols have their usual meanings. The ticks in the remarks column indicate the cleaned and good-quality data available for the analysis. Here, $F_{\rm var}$ is not estimated for the observations affected by high particle background flares and the corresponding columns are filled with '−' symbol. Similarly, Total$_{\rm rms}$ is not estimated when PDS is modelled only with a `constant` component and for such cases, respective column is filled using '−'. See the text for details.

Source	Mission	ObsID	Epoch	Date	MJD	Exposure (ks)	Rate (cts/s) (0.3 − 10 keV)	$F_{\rm var}$	Total$_{\rm rms}$ (%)	Remarks
NGC 55 ULX1	*XMM-Newton*	0028740201	XMM1	2001-11-14	52227.63	30.4	1.80 ± 0.23	16.39 ± 1.84	24.11 ± 2.88	✓
		0028740101	XMM2	2001-11-15	52228.05	26.1	1.94 ± 0.33	21.09 ± 2.38	22.61 ± 0.92	✓
		0655050101	XMM3	2010-05-24	55340.32	113.7	0.91 ± 0.16	10.16 ± 6.15	50.29 ± 1.47	✓
		0824570101	XMM4	2018-11-17	58439.62	108.9	0.66 ± 0.14	5.98 ± 2.23	45.36 ± 1.73	✓
		0852610101	XMM5	2019-11-27	58814.87	4.7	1.69 ± 0.23	10.02 ± 1.32	–	✓
		0852610201	XMM6	2019-12-27	58844.52	4.8	1.72 ± 0.24	9.80 ± 1.44	–	✓
		0852610301	XMM7	2020-05-11	58980.93	5.8	0.70 ± 0.15	9.34 ± 3.94	–	✓
		0852610401	XMM8	2020-05-19	58988.40	4.8	1.66 ± 0.34	12.22 ± 3.14	–	✓
		0864810101	XMM9	2020-05-24	58993.92	117.7	0.92 ± 0.16	16.42 ± 6.29	45.79 ± 3.16	✓
		0883960101	XMM10	2021-12-12	59560.31	130	1.14 ± 0.11	5.65 ± 2.75	48.21 ± 13.77	✓
NGC 4395 ULX1	*XMM-Newton*	0112521901	XMM1	2002-05-31	52425.03	13.9	0.27 ± 0.09	9.03 ± 3.18	–	Poor statistics
		0112522001	XMM2	2002-06-12	52437.76	17.1	–	–	–	Obs. affected by particle flares
		0112522701	XMM3	2003-01-03	52642.93	6.7	0.29 ± 0.09	11.23 ± 8.24	–	Poor statistics
		0142830101	XMM4	2003-11-30	52973.14	103.4	0.33 ± 0.11	4.11 ± 1.19	44.22 ± 5.18	✓
		0744010101	XMM5	2014-12-28	57019.42	53.5	–	–	–	Source is offset in CCD frame
		0744010201	XMM6	2014-12-30	57021.42	53	–	–	–	Source is offset in CCD frame
		0824610101	XMM7	2018-12-13	58465.26	112.8	0.40 ± 0.12	16.83 ± 6.87	25.65 ± 3.32	✓
		0824610201	XMM8	2018-12-19	58471.24	113.6	0.47 ± 0.11	81.17 ± 4.59	41.55 ± 2.13	✓
		0824610301	XMM9	2018-12-31	58483.22	110.5	0.38 ± 0.27	93.85 ± 57.71	45.18 ± 6.28	✓
		0824610401	XMM10	2019-01-02	58485.21	105.9	0.76 ± 0.16	25.67 ± 6.64	36.54 ± 5.64	✓
		0913600101	XMM11	2022-12-10	59923.34	33	0.31 ± 0.07	12.74 ± 4.36	37.78 ± 12.22	✓
		0913600501	XMM12	2022-12-14	59927.98	30	0.31 ± 0.16	10.65 ± 5.24	35.58 ± 6.53	✓
		0913600601	XMM13	2022-12-19	59932.32	38.8	0.22 ± 0.07	15.57 ± 5.38	39.04 ± 12.93	✓
		0913600701	XMM14	2022-12-22	59935.65	28	0.26 ± 0.06	7 ± 4	40.38 ± 17.66	✓
		0913600801	XMM15	2022-12-26	59939.86	28	0.24 ± 0.08	8.14 ± 1.58	32.23 ± 7.93	✓
		0913600901	XMM16	2022-12-30	59943.59	28	–	–	–	Obs. affected by particle flares
		0932391701	XMM17	2024-06-01	60462.76	43	0.26 ± 0.05	8.28 ± 4.07	39.57 ± 7.02	✓
		0932391801	XMM18	2024-06-02	60463.69	36	–	–	–	Obs. affected by particle flares
NGC 5204 X-1	*XMM-Newton*	0142770101	XMM1	2003-01-06	52645.05	16.9	0.66 ± 0.13	4.90 ± 1.38	–	✓
		0142770301	XMM2	2003-04-25	52754.57	$\lesssim 1$	–	–	–	Low exposure data
		0150650301	XMM3	2003-05-01	52760.18	2.9	1.11 ± 0.17	4.16 ± 3.13	28.41 ± 1.62	✓
		0405690101	XMM4	2006-11-15	54054.85	1.9	1.37 ± 0.19	~ 0.42	–	✓
		0405690201	XMM5	2006-11-19	54058.84	35.7	1.13 ± 0.18	5.11 ± 1.23	36.45 ± 7.38	✓
		0405690501	XMM6	2006-11-25	54064.82	15.9	0.83 ± 0.14	5.25 ± 1.42	46.96 ± 3.73	✓
		0693851401	XMM7	2013-04-21	56403.21	15	0.66 ± 0.13	7.64 ± 6.57	–	✓
		0693850701	XMM8	2013-04-29	56411.19	11.3	0.70 ± 0.13	5.01 ± 1.22	–	✓
		0741960101	XMM9	2014-06-27	56835.95	21.3	0.64 ± 0.13	2.04 ± 1.12	–	✓
		0921360101	XMM10	2023-05-18	60082.92	123	0.77 ± 0.15	2.74 ± 1.12	43.51 ± 7.88	✓
		0921360201	XMM11	2023-11-10	60258.43	122	0.95 ± 0.21	4.82 ± 1.78	32.44 ± 8.72	✓
NGC 4190 ULX1	*XMM-Newton*	0654650101	XMM1	2010-06-06	55353.51	21.1	–	–	–	Obs. affected by particle flares
		0654650201	XMM2	2010-06-08	55355.47	9.8	1.05 ± 0.17	4.29 ± 1.82	–	✓
		0654650301	XMM3	2010-11-25	55525.06	5.8	1.77 ± 0.25	6.53 ± 1.12	–	✓

3 RESULTS

3.1 Timing Analysis

3.1.1 Variability and Hardness-Intensity Diagram (HID)

We study the variability properties of all the sources considered in this work. First, we generate background subtracted 200 s binned *EPIC-PN* light curves in $0.3 - 10$ keV energy range. Next, to deduce the variability properties of the sources, we calculate the fractional rms variability amplitude, $F_{\rm var} = \frac{\sqrt{S^2 - \overline{\sigma^2_{err}}}}{\overline{x}}$ following Vaughan et al. (2003); Bhuvana et al. (2021). Here, $\overline{x}$, S^2 and $\overline{\sigma^2_{err}}$ are the mean count rate, variance, and associated error of the light curve. We find that the sources exhibit distinct variability properties with $F_{\rm var}$ varying in a wide range of $4.11 - 93.85\%$ including all the four sources and NGC 4395 ULX1 remains the most variable source (see Table 1). Note that, a similar study on the BH-ULX variability indicates $F_{\rm var} \sim 1.42 - 27.28\%$ for the rest of the five sources (see Paper-I). In Fig. 1(a)-(b), we depict the background subtracted 200 s binned light curves of NGC 55 ULX1 and NGC 4395 ULX1, respectively, for the representation of variability in BH-ULXs. It is noteworthy that for most of the sources marginal variability is observed and hence we refrain from presenting the light curves of the remaining sources in Fig. 1.

Further, we generate the hardness-intensity diagram (HID) by defining the hardness ratio as $HR = C_1/C_2$ with C_1 and C_2 being the background subtracted count rates in $2 - 10$ keV and $0.3 - 2$ keV energy ranges, respectively. In Fig. 1c, the HID of the respective sources are presented using different colored open circles. The data points in the HID of NGC 6946 X−1, NGC 1313 X−1, IC 342 X−1 and NGC 5408 X−1 are adopted from the results presented in Paper-I for comparison. We observe that each source shows a distinct pattern in the HID. In particular, NGC 55 ULX1 and NGC 5408 X−1 roughly show $HR \lesssim 0.15$ and IC 342 X−1 exhibit a relatively harder nature with $HR \sim 1$, whereas the rest of the sources remain confined within $0.15 \lesssim HR \lesssim 0.6$

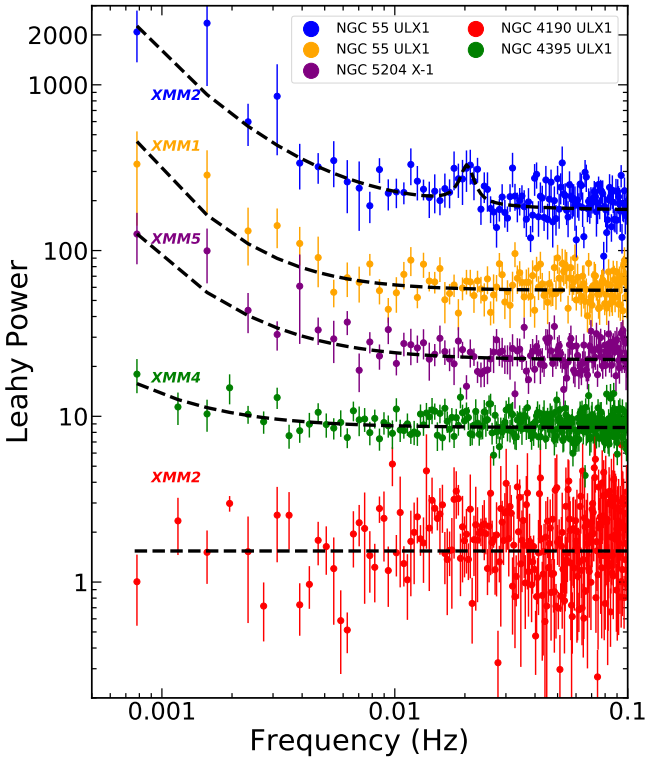

Figure 2. The PDS of NGC 55 ULX1, NGC 5204 X−1, NGC 4395 ULX1 and NGC 4190 ULX1 are depicted with different colors in respective Epochs. Each PDS is fitted with the combination of `constant`, `powerlaw`, and `Lorentzian` components as needed. The powers corresponding to the first four PDS presented from top to bottom are re-scaled with the constant multiplicative factors of 100, 32, 12, and 4.5, respectively, for better clarity. See the text for details.

in the HID. We observe that the HIDs of NGC 55 ULX1 and NGC 4395 ULX1 differ from the other sources, as they coarsely exhibit a 'C-shaped' pattern (see Fig. 1c). Indeed, three of the most recent observations of NGC 4395 ULX1 show fainter characteristics at higher energies ($\gtrsim$ 2 keV) (see §4.2) and remain as outlier ($HR \sim 0.07$) from the 'C-shaped' pattern in the HID. Note that the intensity of these two sources varies significantly with HR, whereas the remaining sources do not show such variations. On the other hand, an apparent negative correlation is observed between HR and the count rate of NGC 5204 X−1, NGC 1313 X−1 and IC 342 X−1, respectively.

3.1.2 Power Density Spectra

The power spectral properties including QPO features are extensively studied for the five BH-ULXs namely NGC 1313 X−1, NGC 5408 X−1, M82 X−1, NGC 6946 X−1 and IC 342 X−1 in Paper-I. Following a similar approach, we investigate the power density spectrum (PDS) of the observations for the remaining four sources (NGC 55 ULX1, NGC 5204 X−1, NGC 4395 ULX1 and NGC 4190 ULX1) using *EPIC-PN* data in 0.3 − 10 keV energy range. The PDS of the individual sources show a constant Poisson noise power within 1.64 − 1.96 and a power-law distribution towards the low-frequency, which are modeled with a `constant` and `powerlaw` components, respectively. However, no significant variability is seen for a few observations of the sources (see Table 1), and a `constant` component is found to be sufficient to fit the PDS. In Fig. 2, we depict the PDS of the sources in different colors for respective Epochs. Further, we estimate the total percentage rms amplitude of the PDS in the 0.001 − 0.1 Hz frequency range for the individual sources and find it to vary within 22.61 − 50.29%.

- *Possible detection of QPO:* Interestingly, we notice that in one of the observation (XMM2) of NGC 55 ULX1, significant excess in power remains near $\sim$ 0.02 Hz after fitting the continuum with a `powerlaw` and `constant` components for a $\chi^2_{\rm red}$ of 167/125 = 1.34. Hence, to fit the observed feature, we include one `Lorentzian` component near $\sim$ 0.02 Hz. In general, each `Lorentzian` component is defined with three parameters namely the centroid frequency (LC), width (LW) and normalization (LN). With this, the resultant fit is obtained for an improved $\chi^2_{\rm red}$ of 156/122 = 1.28 with the best-fitted `Lorentzian` centroid frequency of $20.43^{+1.26}_{-1.67}$ mHz. Next, we calculate the significance ($LN/err_{\rm neg}$, where, $err_{\rm neg}$ being the negative error in normalization), rms amplitude and Quality factor ($Q = LC/LW$) (Belloni et al. 2012; Sreehari et al. 2019; Majumder et al. 2022, 2023) of the fitted feature and obtained as 2.8σ, 6.63% and 6.68, respectively. Based on the observed high Q-factor and strength of the feature ($rms\% \sim 6.63$), we interpret it as the possible detection of a QPO characteristics in NGC 55 ULX1. For the remaining observations of the respective sources, power spectra remain featureless without any detection of QPO.

3.2 Spectral Analysis

3.2.1 Spectral Modeling

We model the *XMM-Newton* spectra in 0.3 − 10 keV energy range of all the available observations for each source using `XSPEC V12.13.1` (Arnaud 1996) in `HEASOFT V6.32.1`. The necessary background spectra, instrument response and ancillary files are also used while doing the spectral modeling. Both *EPIC-PN* and *EPIC-MOS* spectra are simultaneously fitted by including a `constant` component to adjust the calibration offset between the instruments. It is worth mentioning that the individual spectra of *EPIC-PN*, *EPIC-MOS1* and *EPIC-MOS2* are not combined for spectral fitting.

In the modeling, we consider the model combination, `constant`×`Tbabs`×(`diskbb`+`nthComp`), comprising of a thermal Comptonization component (`nthComp` in `XSPEC`) (Zdziarski et al. 1996) and a standard disc component (`diskbb` in `XSPEC`) (Makishima et al. 1986). Here, `Tbabs` takes care of the inter-galactic absorption column and the absorption local to the source (Wilms et al. 2000). It is worth mentioning that a similar model formalism is found to provide the best fit of the *XMM-Newton* spectra for other four sources (NGC 5408 X−1, NGC 1313 X−1, NGC 6946 X−1 and IC 342 X−1) as presented in Majumder et al. (2023). Hence, we proceed to generalize the model prescription for all the BH-ULXs considered in this work. While doing so, the seed photon temperature of `nthComp` component kept tied with the inner disc temperature of the `diskbb` component during the spectral modeling. With this, the above model

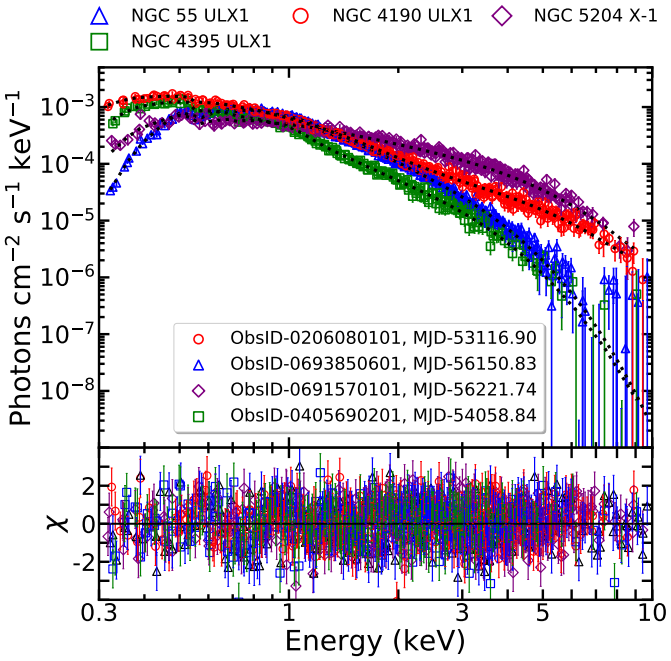

Figure 3. Top: Best fitted *EPIC-PN* and *EPIC-MOS* energy spectra of the four sources plotted simultaneously in $0.3-10$ keV energy range. Each spectrum is modeled using the model combination `constant`×`Tbabs`×(`diskbb`+`nthComp`). Bottom: Variation of residuals (in units of σ) obtained from the best fit of the individual spectra. See the text for details.

prescription is seen to provide the best fit for the observations of all the sources under consideration. The best-fitted model parameters and the corresponding fit statistics are tabulated in Table 2 for NGC 55 ULX1, NGC 5204 X−1, NGC 4395 ULX1 and NGC 4190 ULX1. We mention that the disc contribution is observed to be negligible and the Comptonization component remains adequate to delineate the spectra in a few observations (see Table 2). In contrast, we notice that for a few observations (XMM11−XMM17) of NGC 4395 ULX1, the disc component alone remains adequate to fit the spectra. This is mostly because of the extremely faint nature of the source in higher energies ($\gtrsim 2$ keV) during these observations in which high-quality data remains up to $\lesssim 2$ keV only for spectral modeling. Additionally, we notice that the electron temperature remains unconstrained in most of the observations and hence, frozen to the best-fitted values. Notably, in a few observations (XMM1, XMM3, XMM4, XMM9) of NGC 55 ULX1, an absorption `edge` is required to adjust the residuals near ~ 1 keV (Jithesh 2022). In contrast, a `Gaussian` line is used to fit the broad emission feature observed at ~ 1 keV in all the spectra of NGC 4395 ULX1 (Ghosh et al. 2022). The best-fitted energy spectra of NGC 55 ULX1, NGC 4395 ULX1, NGC 5204 X−1 and NGC 4190 ULX1 are shown in Fig. 3 for the purpose of representation. Further, we compute the flux associated with different model components, optical depth, and Compton y-parameter following Paper-I. Also, the total and disc bolometric luminosities are estimated from the flux values, assuming the well-constrained source distances (see Table 2).

3.2.2 *Spectral Properties*

In general, spectral features of the sources are well described by standard accretion disc and thermal Comptonization components, very similar to the spectral morphologies of a group of BH-ULXs presented in Paper-I. We find that the spectral modeling results the photon index ($\Gamma_{\rm nth}$) in the range of $1.66^{+0.13}_{-0.06}-3.86^{+0.25}_{-0.29}$ and the inner disc temperature ($kT_{\rm in}$) varies within $0.14^{+0.01}_{-0.01}-0.32^{+0.02}_{-0.02}$ keV for NGC 55 ULX1, NGC 4395 ULX1, NGC 5204 X−1 and NGC 4190 ULX1 (see Table 2). Note that, similar model formalism, used to fit the spectra of the remaining sources (NGC 1313 X−1, NGC 5408 X−1, NGC 6946 X−1 and IC 342 X−1), results in the electron temperature ($kT_{\rm e}$), $\Gamma_{\rm nth}$ and $kT_{\rm in}$ in the range of $1.62-3.76$ keV, $1.48-2.65$ and $0.16-0.54$ keV, respectively (see Paper-I for details). Further, the optical depth and Compton y-parameter are found to be within $6 \lesssim \tau \lesssim 20$ and $0.46 \lesssim$ y-par $\lesssim 6.24$ considering all the sources (see Table 2 and Paper-I). This suggests that the presence of relatively cool accretion disc and optically thick corona are the generic features of the BH-ULXs considered for this work (Gladstone et al. 2009).

3.2.3 *Spectral Correlation*

In this section, we attempt to deduce intrinsic correlations among the best-fitted and estimated spectral parameters for the respective sources. In doing so, we use the results obtained from the spectral analysis (see §3.2.1) of NGC 55 ULX1, NGC 5204 X−1 and NGC 4395 ULX1, presented in Table 2 along with the findings reported from the detailed spectral modeling of four BH-ULXs (NGC 1313 X−1, NGC 5408 X−1, NGC 6946 X−1, IC 342 X−1) in Paper-I (see Table-4). We investigate the correlation between the bolometric disc luminosity ($L_{\rm disc}$) and color-corrected disc temperature ($T_{\rm col}$) of the respective sources. Note that, the inner disc temperature ($T_{\rm in}$) is multiplied with the spectral hardening factor ($f_{\rm c}=1.7$) following Done & Davis (2008); Davis & El-Abd (2019) to obtain the $T_{\rm col}$. In Fig. 4, we present the obtained results, where, the $L_{\rm disc}$ (in $\times 10^{40}$ erg s^{-1}) is plotted as a function of $T_{\rm col}$ (in keV).

We notice the trend of possible correlations of distinct characteristics between $L_{\rm disc}$ and $T_{\rm col}$ for all the sources. To deduce the firmness of the correlations, we estimate the Pearson correlation coefficient (ρ) of the distributions in $L_{\rm disc}-T_{\rm col}$ plane for the respective cases (see Paper-I). It is found that the source NGC 55 ULX1 shows a negative correlation between $L_{\rm disc}$ and $T_{\rm col}$ with $\rho \sim -0.74$. However, the variation in $L_{\rm disc}$ is found to be marginal for NGC 4395 ULX1 and the corresponding distribution in the $L_{\rm disc}-T_{\rm col}$ plane appears to form two distinct regimes of lower and higher temperatures (see Fig. 4), indicating no evidence of correlation with $\rho \sim -0.11$ only. It may be noted that the higher disc temperatures (~ 0.3 keV) are obtained for the observations in which only the disc component fits the entire spectra of narrow energy coverage ($\sim 0.3-2$ keV) in NGC 4395 ULX1. Therefore, the two distinct regions of different disc temperatures (see Fig. 4) perhaps resulted from the difference in model prescriptions for the respective cases. Contrarily, NGC 5204 X−1 is seen to exhibit a clear positive correlation with $\rho \sim +0.7$. Moreover, a strong negative correlation is obtained with $\rho \sim -0.81$ for the combined results

Table 2. Best-fitted and estimated spectral parameters obtained from the simultaneous modeling of *EPIN-PN* and *EPIN-MOS* spectra of the *XMM-Newton* observations of respective sources in 0.3 − 10 keV energy range using the model combination `constant×TBabs×(diskbb + nthComp)`. All the quantities mentioned in the table have their usual meanings. The flux and luminosity values are presented in units of $\times 10^{-12}$ erg cm^{-2} s^{-1} and $\times 10^{39}$ erg s^{-1}, respectively.

Parameters	XMM1	XMM2	XMM3	XMM4	XMM5	XMM6	XMM7	XMM8	XMM9	XMM10	XMM11
					NGC 55 ULX1						
					(D = 1.94 Mpc)						
$n_{\rm H}$ (10^{22} cm^{-2})	$0.16^{+0.04}_{-0.03}$	$0.33^{+0.05}_{-0.06}$	$0.11^{+0.02}_{-0.02}$	$0.15^{+0.03}_{-0.03}$	$0.38^{+0.04}_{-0.04}$	$0.41^{+0.12}_{-0.08}$	$0.43^{+0.12}_{-0.13}$	$0.40^{+0.11}_{-0.18}$	$0.11^{+0.02}_{-0.02}$	0.11*	–
$kT_{\rm in}$ (keV)	–	$0.16^{+0.02}_{-0.03}$	–	–	$0.15^{+0.03}_{-0.03}$	$0.14^{+0.03}_{-0.02}$	$0.14^{+0.01}_{-0.01}$	$0.15^{+0.03}_{-0.04}$	–	–	–
$\Gamma_{\rm nth}$	$3.01^{+0.06}_{-0.05}$	$2.65^{+0.02}_{-0.05}$	$3.64^{+0.07}_{-0.07}$	$3.42^{+0.05}_{-0.06}$	$3.27^{+0.08}_{-0.07}$	$3.31^{+0.15}_{-0.13}$	$3.32^{+0.21}_{-0.30}$	$3.31^{+0.26}_{-0.33}$	$3.56^{+0.08}_{-0.07}$	$3.48^{+0.04}_{-0.04}$	–
$kT_{\rm e}$ (keV)	1.62*	1.62*	1.62*	2*	1.89*	1.62*	2*	2*	1.62*	2*	–
χ^2/d.o.f	338/283	383/261	470/319	422/312	207/169	164/145	152/107	99/96	456/337	476/287	–
$F_{\rm disc}$	–	2.88 ± 0.19	–	–	5.36 ± 0.49	9.03 ± 0.41	4.95 ± 0.34	7.40 ± 0.34	–	–	–
$F_{\rm nth}$	6.21 ± 0.14	8.39 ± 0.18	2.89 ± 0.07	2.60 ± 0.06	9.32 ± 0.21	10.04 ± 0.52	3.63 ± 0.17	5.10 ± 0.23	2.88 ± 0.19	4.71 ± 0.04	–
$F_{\rm bol}$	7.46 ± 0.17	16.04 ± 0.36	3.57 ± 0.08	3.39 ± 0.08	23.62 ± 0.54	33.78 ± 0.75	16.21 ± 0.72	21.76 ± 1.47	3.58 ± 0.08	4.75 ± 0.03	–
$L_{\rm bol}$	3.36 ± 0.08	7.22 ± 0.16	1.60 ± 0.04	1.53 ± 0.04	10.64 ± 0.24	15.21 ± 0.33	7.30 ± 0.32	9.81 ± 0.66	1.61 ± 0.06	2.14 ± 0.01	–
$L_{\rm disc}$	–	2.44 ± 0.09	–	–	4.58 ± 0.22	8.10 ± 0.18	4.89 ± 0.16	6.51 ± 0.15	–	–	–
τ	8.32 ± 0.21	9.72 ± 0.23	6.62 ± 0.15	6.30 ± 0.13	6.88 ± 0.21	7.42 ± 0.41	6.53 ± 0.72	6.55 ± 0.79	6.80 ± 0.18	6.16 ± 0.08	–
y-par	0.88 ± 0.04	1.19 ± 0.06	0.55 ± 0.03	0.62 ± 0.03	0.70 ± 0.04	0.69 ± 0.08	0.67 ± 0.15	0.67 ± 0.16	0.58 ± 0.03	0.59 ± 0.02	–
					NGC 5204 X−1						
					(D = 4.8 Mpc)						
$n_{\rm H}$ (10^{22} cm^{-2})	$0.04^{+0.02}_{-0.02}$	–	$0.05^{+0.03}_{-0.02}$	$0.06^{+0.01}_{-0.02}$	$0.06^{+0.01}_{-0.01}$	$0.04^{+0.01}_{-0.01}$	$0.06^{+0.03}_{-0.03}$	$0.04^{+0.01}_{-0.01}$	$0.04^{+0.02}_{-0.02}$	$0.06^{+0.01}_{-0.01}$	$0.07^{+0.01}_{-0.01}$
$kT_{\rm in}$ (keV)	$0.26^{+0.04}_{-0.02}$	–	$0.28^{+0.06}_{-0.06}$	$0.29^{+0.05}_{-0.03}$	$0.28^{+0.03}_{-0.03}$	$0.28^{+0.03}_{-0.03}$	$0.24^{+0.04}_{-0.04}$	$0.25^{+0.05}_{-0.04}$	$0.25^{+0.04}_{-0.03}$	$0.24^{+0.01}_{-0.01}$	$0.25^{+0.03}_{-0.02}$
$\Gamma_{\rm nth}$	$1.66^{+0.13}_{-0.06}$	–	$2.07^{+0.14}_{-0.16}$	$2.16^{+0.29}_{-0.11}$	$2.12^{+0.15}_{-0.16}$	$1.85^{+0.11}_{-0.12}$	$1.69^{+0.11}_{-0.09}$	$1.77^{+0.13}_{-0.16}$	$1.76^{+0.09}_{-0.11}$	$1.79^{+0.05}_{-0.05}$	$2.17^{+0.12}_{-0.12}$
$kT_{\rm e}$ (keV)	$1.62^{+0.38}_{-0.27}$	–	2.5*	1.62*	$2.07^{+1.04}_{-0.42}$	2.65*	$1.73^{+0.49}_{-0.25}$	2.13*	$1.98^{+0.61}_{-0.34}$	$2.09^{+0.29}_{-0.21}$	$2.49^{+0.88}_{-0.43}$
χ^2/d.o.f	236/225	–	167/164	103/133	327/328	319/296	223/212	238/208	268/247	525/395	393/332
$F_{\rm disc}$	0.46 ± 0.02	–	0.68 ± 0.05	0.95 ± 0.02	0.76 ± 0.02	0.57 ± 0.01	0.52 ± 0.02	0.42 ± 0.02	0.37 ± 0.02	0.85 ± 0.02	0.86 ± 0.03
$F_{\rm nth}$	1.29 ± 0.03	–	1.95 ± 0.09	2.27 ± 0.10	2.10 ± 0.05	1.58 ± 0.04	1.35 ± 0.06	1.46 ± 0.07	1.34 ± 0.03	1.76 ± 0.02	2.41 ± 0.02
$F_{\rm bol}$	2.04 ± 0.03	–	3.15 ± 0.07	3.76 ± 0.09	3.37 ± 0.03	2.64 ± 0.06	2.21 ± 0.05	2.24 ± 0.05	2.02 ± 0.05	2.61 ± 0.03	3.24 ± 0.04
$L_{\rm bol}$	5.62 ± 0.08	–	8.69 ± 0.02	10.37 ± 0.03	9.29 ± 0.08	7.31 ± 0.02	6.09 ± 0.14	6.18 ± 0.14	5.57 ± 0.16	7.19 ± 0.05	8.93 ± 0.03
$L_{\rm disc}$	1.71 ± 0.06	–	2.48 ± 0.14	3.45 ± 0.06	2.78 ± 0.06	2.10 ± 0.03	1.98 ± 0.06	1.59 ± 0.06	1.71 ± 0.05	2.34 ± 0.04	2.37 ± 0.05
τ	18.37 ± 3.26	–	10.47 ± 1.11	12.60 ± 1.54	11.27 ± 2.42	11.89 ± 1.14	17.23 ± 3.17	14.33 ± 1.72	15.04 ± 2.35	14.24 ± 1.27	3.31 ± 0.28
y-par	4.27 ± 1.07	–	2.14 ± 0.46	2.01 ± 0.48	2.05 ± 0.42	2.93 ± 0.56	4.01 ± 0.83	3.42 ± 0.82	3.51 ± 0.67	3.31 ± 0.28	1.89 ± 0.28

*Frozen to best-fitted value.

Table 2 – *continued*

Parameters	XMM2	XMM3	XMM4	XMM7	XMM8	XMM9	XMM10	XMM11	XMM12	XMM13	XMM14	XMM15	XMM17
						NGC 4395 ULX1							
						(D = 4.76 Mpc)							
$n_{\rm H}$ (10^{22} cm^{-2})	–	–	$0.10^{+0.03}_{-0.03}$	$0.10^{+0.02}_{-0.02}$	$0.10^{+0.02}_{-0.02}$	$0.11^{+0.03}_{-0.02}$	$0.11^{+0.03}_{-0.02}$	$0.03^{+0.01}_{-0.01}$	0.03*	0.03*	0.04*	0.05*	0.05*
$kT_{\rm in}$ (keV)	–	–	$0.15^{+0.02}_{-0.02}$	$0.15^{+0.02}_{-0.02}$	$0.16^{+0.03}_{-0.03}$	$0.15^{+0.03}_{-0.03}$	–	$0.32^{+0.02}_{-0.02}$	$0.31^{+0.01}_{-0.01}$	$0.31^{+0.01}_{-0.01}$	$0.31^{+0.01}_{-0.01}$	$0.29^{+0.01}_{-0.01}$	$0.31^{+0.01}_{-0.01}$
$\Gamma_{\rm nth}$	–	–	$3.34^{+0.17}_{-0.18}$	$3.33^{+0.18}_{-0.16}$	$3.20^{+0.09}_{-0.08}$	$3.86^{+0.25}_{-0.29}$	$3.05^{+0.05}_{-0.05}$	–	–	–	–	–	–
$kT_{\rm e}$ (keV)	–	–	2*	1.92*	2*	2*	1.62*	–	–	–	–	–	–
$\chi^2/d.o.f$	–	–	179/155	180/155	259/212	179/146	313/237	118/77	96/86	123/82	141/87	127/79	131/108
$F_{\rm disc}$	–	–	0.23 ± 0.02	0.24 ± 0.02	0.24 ± 0.03	0.27 ± 0.03	–	0.55 ± 0.01	0.43 ± 0.01	0.41 ± 0.02	0.52 ± 0.01	0.49 ± 0.01	0.55 ± 0.02
$F_{\rm nth}$	–	–	0.63 ± 0.03	0.62 ± 0.02	1.34 ± 0.03	0.74 ± 0.03	1.81 ± 0.03	–	–	–	–	–	–
$F_{\rm bol}$	–	–	1.37 ± 0.03	1.40 ± 0.03	2.37 ± 0.03	1.76 ± 0.04	2.71 ± 0.04	0.57 ± 0.01	0.45 ± 0.01	0.42 ± 0.02	0.54 ± 0.01	0.51 ± 0.01	0.57 ± 0.02
$L_{\rm bol}$	–	–	3.71 ± 0.08	3.80 ± 0.08	6.43 ± 0.08	4.77 ± 0.11	7.35 ± 0.08	1.55 ± 0.02	1.22 ± 0.01	1.14 ± 0.02	1.46 ± 0.02	1.38 ± 0.01	1.55 ± 0.02
$L_{\rm disc}$	–	–	1.27 ± 0.05	1.31 ± 0.03	1.28 ± 0.04	1.61 ± 0.05	–	1.49 ± 0.02	1.17 ± 0.01	1.11 ± 0.02	1.41 ± 0.02	1.33 ± 0.01	1.49 ± 0.02
τ	–	–	6.48 ± 0.41	6.67 ± 0.44	6.83 ± 0.23	5.43 ± 0.51	8.13 ± 0.16	–	–	–	–	–	–
y-par	–	–	0.66 ± 0.08	0.67 ± 0.09	0.73 ± 0.05	0.46 ± 0.08	0.85 ± 0.03	–	–	–	–	–	–
						NGC 4190 ULX1							
						(D = 3 Mpc)							
$n_{\rm H}$ (10^{22} cm^{-2})	$0.06^{+0.01}_{-0.01}$	$0.15^{+0.06}_{-0.02}$	–	–	–	–	–	–	–	–	–	–	–
$\Gamma_{\rm nth}$	$2.09^{+0.19}_{-0.12}$	$1.69^{+0.03}_{-0.03}$	–	–	–	–	–	–	–	–	–	–	–
$kT_{\rm e}$ (keV)	1.62*	$1.67^{+0.11}_{-0.11}$	–	–	–	–	–	–	–	–	–	–	–
χ^2/d.o.f	317/293	335/337	–	–	–	–	–	–	–	–	–	–	–
$F_{\rm nth}$	3.31 ± 0.06	7.13 ± 0.09	–	–	–	–	–	–	–	–	–	–	–
$F_{\rm bol}$	3.53 ± 0.07	8.17 ± 0.12	–	–	–	–	–	–	–	–	–	–	–
$L_{\rm bol}$	3.80 ± 0.07	8.79 ± 0.13	–	–	–	–	–	–	–	–	–	–	–
τ	13.16 ± 1.61	17.56 ± 0.79	–	–	–	–	–	–	–	–	–	–	–
y-par	2.19 ± 0.53	4.03 ± 0.23	–	–	–	–	–	–	–	–	–	–	–

*Frozen to best-fitted value.

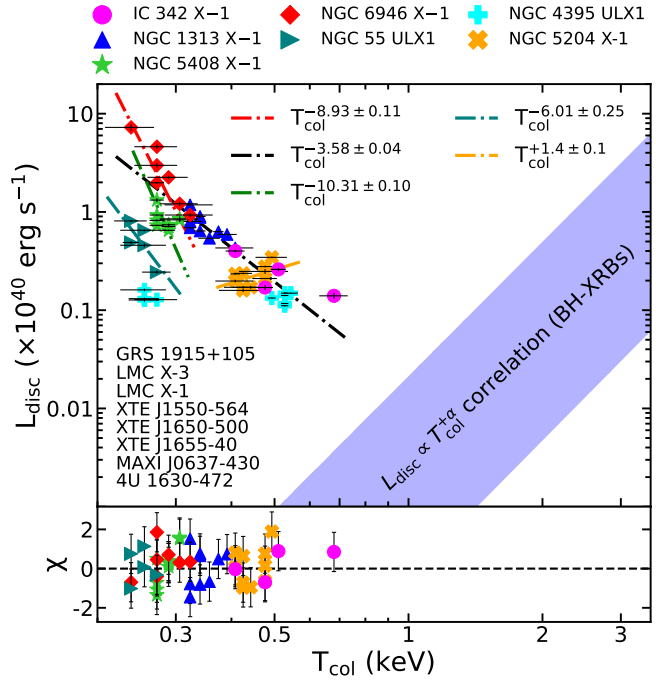

Figure 4. Correlation between the bolometric disc luminosity and color-corrected inner disc temperature of all BH-ULXs. The dash-dot lines of different colors represent the best fit in describing the $L_{\rm disc} - T_{\rm col}$ distribution of each source with the functional form mentioned in the figure. The blue-shaded region represents the correlation between the luminosity and disc temperature of the form $L_{\rm disc} \propto T_{\rm col}^{+\alpha}$ for eight BH-XRBs, adopted from Gierliński & Done 2004; Abe et al. 2005; Vierdayanti et al. 2010; Baby et al. 2021. See the text for details.

of NGC 1313 X−1 and IC 342 X−1, and $\rho \sim -0.89$ for NGC 6946 X−1. Although, we find a weak anti-correlation with $\rho \sim -0.27$ in $L_{\rm disc} - T_{\rm col}$ plane of NGC 5408 X−1.

Further, we proceed to delineate the observed correlations of the sources with the empirical power-law profile $L_{\rm disc} \propto T_{\rm col}^{\alpha}$ (Rybicki & Lightman 1979) using the `curve_fit`[6] module in `Python`. The individual fits result the power-law exponent (α) as -6.01 ± 0.25, -8.93 ± 0.11, -10.31 ± 0.10 and 1.4 ± 0.1 for NGC 55 ULX1, NGC 6946 X−1, NGC 5408 X−1 and NGC 5204 X−1, respectively. However, the combined fitting of the correlation distributions for IC 342 X−1 and NGC 1313 X−1 indicates $\alpha = -3.58 \pm 0.04$. It may be noted that because of the marginal variation observed in $L_{\rm disc}$ and $T_{\rm col}$, we refrain from modeling the luminosity-temperature distribution for NGC 4395 ULX1. In Fig. 4, we present the best-fitted power-law functional form in the top panel for the respective sources and the residuals in the bottom panel, respectively. In addition, we show the positive correlation between the disc luminosity and temperature of the form $L_{\rm disc} \propto T_{\rm col}^{+\alpha}$, typically observed for BH-XRBs, with a blue shade in Fig. 4. Note that the data associated with these correlation properties are adopted from Gierliński & Done (2004); Abe et al. (2005); Vierdayanti et al. (2010); Baby et al. (2021) and the disc temperature values are color-corrected using the same hardening factor ($f_{\rm c} = 1.7$), considered for the present work.

[6] https://docs.scipy.org/doc/scipy/reference/generated/scipy.optimize.curve_fit.html

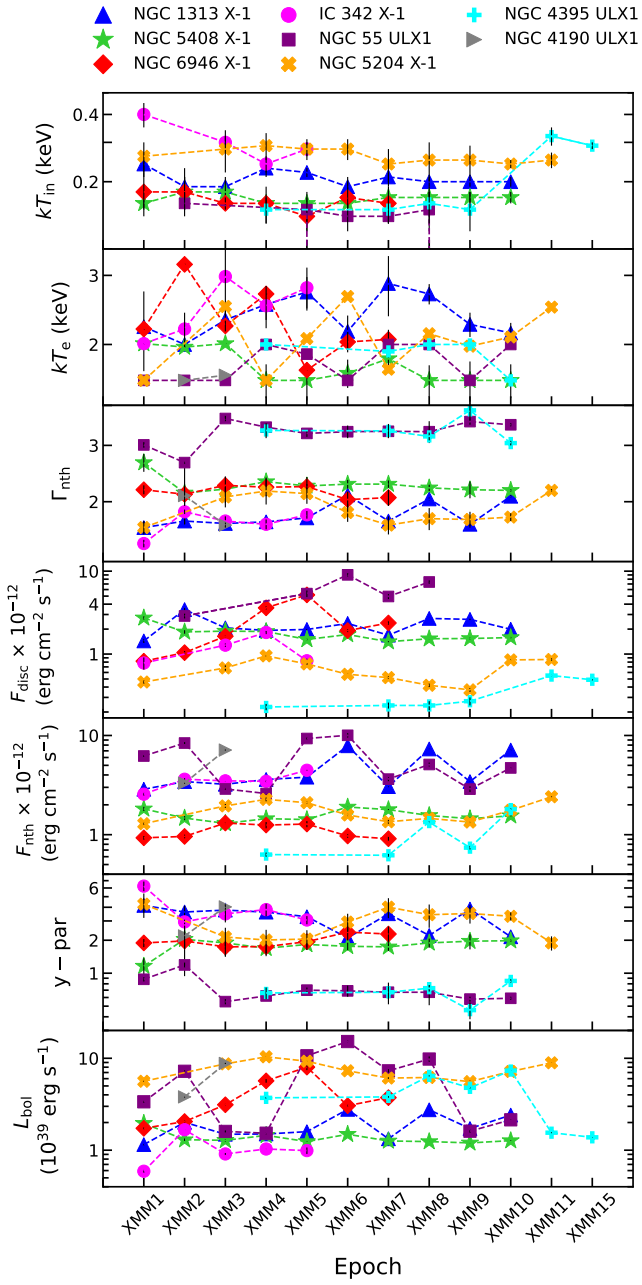

Figure 5. Evolution of the spectral parameters over the long-term monitoring are shown with distinct colored markers for the respective sources. The variation of inner disc temperature, electron temperature, photon index, disc flux, Comptonized flux, Compton y-parameter and bolometric luminosity over different Epochs are shown from top to bottom panels, respectively. See the text for details.

3.2.4 *Evolution of Spectral Properties*

We study the long-term spectral evolution of the eight BH-ULXs namely NGC 1313 X−1, IC 342 X−1, NGC 4395 ULX1, NGC 5408 X−1, NGC 55 ULX1, NGC 4190 ULX1,

NGC 6946 X−1 and NGC 5204 X−1 using the *XMM-Newton* observations over a decade. In Fig. 5, the variation of inner disc temperature ($kT_{\rm in}$ in keV), electron temperature ($kT_{\rm e}$ in keV), photon index ($\Gamma_{\rm nth}$), disc flux ($F_{\rm disc}$ in erg cm^{-2} s^{-1}), Comptonized flux ($F_{\rm nth}$ in erg cm^{-2}s^{-1}), Compton y-parameter (y-par) and bolometric luminosity ($L_{\rm bol}$ in erg s^{-1}) are depicted from top to bottom panels, respectively, over different Epochs of observation. We mention that the best-fitted spectral parameters of NGC 1313 X−1, IC 342 X−1, NGC 5408 X−1, and NGC 6946 X−1 are adopted from the results presented in Paper-I (see Table-4 of the paper). However, for the rest of the sources, the best-fitted parameters are tabulated in Table 2.

We observe that the spectral properties of the BH-ULXs generally exhibit significant variation over the long-term evolution of the sources and manifest several spectral states. In particular, we find the dominance of the Comptonization flux over the disc contribution ($F_{\rm nth} \gtrsim F_{\rm disc}$) for NGC 5204 X−1, IC 342 X−1, NGC 4190 ULX1 and NGC 1313 X−1, respectively. As expected, the photon index is observed to be in the harder limit of $\Gamma_{\rm nth} \lesssim 2$, and the y-par, indicative of the amount of Comptonization, remains $\gtrsim 2$ for all the four sources (see Fig. 5). Further, we find a low disc temperature ($kT_{\rm in} \lesssim 0.3$ keV) for these sources except NGC 4190 ULX1 in which the disc is absent and Comptonization contribution is noticeably high. In contrast, NGC 6946 X−1 manifests disc dominated spectral characteristics with $F_{\rm disc} \gtrsim F_{\rm nth}$ and $\Gamma_{\rm nth} \gtrsim 2$ (see Fig. 5). Interestingly, comparable disc and Comptonized flux contributions are seen in the spectra of NGC 55 ULX1 and NGC 5408 X−1. However, the source NGC 55 ULX1 replicates relatively softer nature with $\Gamma_{\rm nth} \gtrsim 3$ and y-par $\lesssim 1$, whereas NGC 5408 X−1 remains in the intermediate regime ($F_{\rm disc} \approx F_{\rm nth}$, $\Gamma_{\rm nth} \lesssim 2$ and $1 <$ y-par $\lesssim 2$). Finally, for NGC 4395 ULX1, we observe a negligible disc contribution with y-par $\lesssim 1$ and high photon index ($\Gamma_{\rm nth} \gtrsim 3$). This possibly resulted from the appearance of broad emission feature at lower energy (~ 1 keV), suggesting distinct and rather complex spectral characteristics of NGC 4395 ULX1. Note that, the spectral parameters of NGC 4395 ULX1 show marginal variations during later epochs (XMM11−XMM17) (see Fig. 2), hence we present only the results for XMM11 and XMM15 in Fig. 5. A significant variation in the luminosity is noticed over the entire observation period of more than a decade for most of the sources. Note that, a low electron temperature within 1 keV $\lesssim kT_{\rm e} \lesssim 3$ keV is obtained for all the sources, indicating the presence of a relatively cool Compton corona, generally seen in ULXs.

4 DISCUSSION

In this work, we study the long-term evolution of the spectro-temporal properties of eight BH-ULXs using *XMM-Newton* observations spanning over a decade or more. The detailed spectral analyses reveal the presence of significant correlations between the color-corrected inner disc temperature ($T_{\rm col}$) and the associated disc luminosity ($L_{\rm disc}$) of the sources. The long-term spectral evolution study infers different spectral states seems to be connected with the observed correlation properties of the respective sources.

We investigate the variability properties of four BH-ULXs, namely NGC 55 ULX1, NGC 4395 ULX1, NGC 5204 X−1 and NGC 4190 ULX1 in detail. For these sources, the fractional variability amplitude is found to vary as 4.11 − 93.85%. A similar study for the remaining sources (*i.e.*, NGC 1313 X−1, NGC 5408 X−1, NGC 6946 X−1 and IC 342 X−1) were already carried out in Paper-I (Majumder et al. 2023), where the fractional variability is obtained as 1.42 − 27.28%. The HID presented in Fig. 1c indicates an apparent anti-correlation between the count rate and HR for NGC 5408 X−1, NGC 1313 X−1, NGC 5204 X−1 and IC 342 X−1, respectively. Further, the power spectral study reveals the total percentage rms variability amplitude as $22 - 50\%$ in $0.001 - 0.1$ Hz frequency range for all BH-ULXs under consideration.

Furthermore, a detailed PDS investigation reveals the detection of a moderately significant ($\sigma \sim 2.8$, $rms\% \sim 6.63$) QPO-like feature at ~ 20 mHz in NGC 55 ULX1 during Epoch XMM2. Interestingly, for this source, the PDS resembles the characteristics of a QPO (see §3.1), although such feature is not observed within a day during its previous observation. It is worth mentioning that NGC 1313 X−1, NGC 5408 X−1, NGC 6946 X−1, M82 X−1 and IC 342 X−1 manifest prominent QPO features of frequency $\sim 8 - 667$ mHz over different observation Epochs of *XMM-Newton* (Atapin et al. 2019; Majumder et al. 2023, and references therein).

4.1 Long-term Evolution of BH-ULXs

The long-term evolution of spectral properties and the flux contributions from different spectral components confirm the presence of soft, intermediate, and hard spectral states in the BH-ULXs. In particular, we observe that NGC 5204 X−1, IC 342 X−1, NGC 4190 ULX1 and NGC 1313 X−1 remain within the group of ULXs, showing harder spectral features with dominant effects of thermal Comptonization (y-par $\gtrsim 2$) and relatively weak disc emission ($F_{\rm disc} \lesssim F_{\rm nth}$) (see Table 2 and Fig. 5). Moreover, the flatter photon index ($\Gamma_{\rm nth} \lesssim 2$) possibly indicates the presence of a Comptonizing tail similar to BH-XRBs spectra in their hard/intermediate states (Remillard & McClintock 2006). With this, we infer that for these BH-ULXs, an optically thick Comptonizing corona residing at the inner region of a low-temperature ($0.2 \lesssim kT_{\rm in} \lesssim 0.4$) disc appears to be the preferred accretion scenario with harder spectral characteristics.

In contrast, we find disc-dominated spectral morphologies in NGC 6946 X−1, where the disc flux is roughly twice the Comptonized flux and $\Gamma_{\rm nth} \gtrsim 2$. Indeed, such classification of the sources based on the spectral flux contribution is similar to the soft-ultraluminous (SUL) and hard-ultraluminous (HUL) states (Sutton et al. 2013). Notably, NGC 6946 X−1 is observed in the disc-dominated state in the absence of a high-energy spectral break in most of the previous studies, and has been identified as a persistent ULX with softer characteristics (Earnshaw et al. 2019; Ghosh & Rana 2023). Finally, the intermediate spectral nature ($F_{\rm disc} \approx F_{\rm nth}$, $\Gamma_{\rm nth} \lesssim 2$ and $1 <$ y-par $\lesssim 2$) is observed for NGC 5408 X−1 over the long-term monitoring which is identified as the intermediate-ultraluminous (IUL) state, whereas NGC 55 ULX1 remains in the SUL state. We note that the presence of a 'bright hard intermediate state' is reported for NGC 5408 X−1 (Caballero-García et al. 2013)

and NGC 55 ULX1 is found to manifest a steep photon index ($\Gamma > 3$) in the previous studies (Jithesh 2022) which are consistent with the present findings.

4.2 Correlation between $L_{\rm disc}$ and $T_{\rm col}$ in BH-ULXs

The variation of $L_{\rm disc}$ with $T_{\rm col}$ affirms the distinct correlation for all the BH-ULXs under consideration. In particular, all the sources, except NGC 5204 X−1, show a negative correlation in the $L_{\rm disc} - T_{\rm col}$ plane, while a clear positive correlation is observed for NGC 5204 X−1. The best-fitted correlations with the empirical power-law distribution $L_{\rm disc} \propto T_{\rm col}^{\alpha}$ yields the exponent as $\alpha = -8.93$ (NGC 6946 X−1), -6.01 (NGC 55 ULX1), -10.31 (NGC 5408 X−1), $+1.4$ (NGC 5204 X−1) and -3.58 (combined IC 342 X−1 and NGC 1313 X−1), respectively (see Fig. 4). It is noteworthy that NGC 4395 ULX1 manifests marginal variation in the disc luminosity and temperature over different observations with $\rho \sim -0.11$ only, and hence we discard it from the present discussion.

We further note that a negative correlation between $L_{\rm disc}$ and $T_{\rm col}$ yielding a power-law exponent of -3.5 is reported for several ULXs (Kajava & Poutanen 2009) that remains consistent with the present study. Interestingly, we observe an apparent connection between the correlation properties and the spectral states of the individual sources. For example, steeper ($\alpha < -4$) anti-correlations are seen for the sources in SUL (NGC 6946 X−1 and NGC 55 ULX1) and IUL (NGC 5408 X−1) spectral states, respectively. However, a more flatter power-law exponent ($\alpha \sim -4$) is noticed for IC 342 X−1 and NGC 1313 X−1 in the HUL state. In addition, NGC 5204 X−1 manifests a positive correlation in the HUL state.

Meanwhile, several galactic BH-XRBs, such as XTE J1550−564, XTE J1650−500, GRO J1655−40, GX 339−4, XTE J1859 + 226 (Gierliński & Done 2004), and MAXI J0637 − 430 (Baby et al. 2021), show clear positive correlations between $L_{\rm disc}$ and $T_{\rm col}$. This is also true for extra-galactic sources like LMC X−1 and LMC X−3 (Gierliński & Done 2004). These correlations align with the predictions of standard disc theory (Shakura & Sunyaev 1973). Interestingly, depending on the luminosity, 4U 1630−472 (Abe et al. 2005), XTE J1550 − 564 (Kubota & Makishima 2004), and GRS 1915 + 105 (Vierdayanti et al. 2010) are observed to follow or deviate from the standard $L_{\rm disc} \propto T_{\rm col}^{4}$ correlation in different observations. In particular, when the luminosity is close to the Eddington limit, the sources are observed to exhibit a flatter correlation of the form $L_{\rm disc} \propto T_{\rm col}^{2}$ (Watarai et al. 2001).

4.3 Possible Dichotomy in $L_{\rm disc} \propto T_{\rm col}^{\alpha}$ Correlation

In this study, we observe both positive and negative correlations in between $L_{\rm disc}$ and $T_{\rm col}$ for all BH-ULXs under consideration. Needless to mention that the appearance of 'unusual' correlation including anti-correlations ('$-\alpha$') leads to the possible dichotomy between the present findings and the existing theoretical frameworks. The BH-XRBs are also seen to deviate from the standard picture on several occasions as pointed out in the preceding section. Nevertheless, several attempts have been made to explain this, although the origin of the dichotomy remains elusive. Depending on α, the correlations are coarsely summarized in three different regimes for several BH-XRBs and BH-ULXs and briefly described as,

$$L_{\rm disc} \propto T_{\rm col}^{\alpha};\quad \begin{cases} \alpha = 4, & \text{(Standard disc)} \\ 0 \leq \alpha < 4, & \text{(Slim disc)} \\ -10 \leq \alpha < 0. & \text{(Anomalous)} \end{cases}$$

- Standard disc scenario: Needless to mention that the luminosity associated with the disc emission is expected to follow $L_{\rm disc} \propto T_{\rm col}^{4}$ as predicted from the standard accretion disc prescription (Shakura & Sunyaev 1973). In general, the Keplerian disc component of the accretion flow locally emits as a multi-color blackbody at different disc radii, resulting in the expected correlation (Frank et al. 2002).
- Slim disc scenario: Several BH-XRBs including 4U 1630 − 472, XTE J1550 − 564 and GRS 1915 + 105 are seen to deviate from the standard disc and mostly follow a flatter correlation as $2 \lesssim \alpha < 4$ (Kubota & Makishima 2004; Abe et al. 2005; Vierdayanti et al. 2010). It has also been suggested that different accretion scenarios exist for these BH-XRBs, which determine the nature of the correlations. In this study, we observe that NGC 5204 X−1 is the only BH-ULX that manifests a positive correlation of the form $L_{\rm disc} \propto T_{\rm col}^{1.4}$, however this relation is not generally determined by the spectral states. Moreover, at relatively higher luminosity, close to the Eddington limit, the deviation from $\alpha \sim 4$ becomes more prominent (Kubota & Makishima 2004). A geometrically thin ($H/r << 1$) and radiatively efficient standard Keplerian disc is characterized with moderately low accretion rate. However, the 'slim disc' appears with relatively higher luminosity ($\gtrsim 0.3 L_{\rm Edd}$) yielding thicker disc geometry ($H/r \lesssim 1$), where the angular momentum remains sub-Keplerian (Abramowicz et al. 1988; Chakrabarti 1995; Beloborodov 1998; Abramowicz & Fragile 2013). Interestingly, a more flatter correlation, *i.e.*, $L_{\rm disc} \propto T_{\rm col}^{2}$, is predicted for such discs (Watarai et al. 2001). Therefore, a possible explanation of the observed anomaly in the deviation of the power-law exponent could be the transition from the standard disc ($\alpha \sim 4$) to the 'slim disc' scenario ($\alpha \sim 2$).
- Anomalous scenario: Intriguingly, the negative correlations with $\alpha < 0$ observed in several BH-ULXs offer challenges, with only a few attempts made to explain these findings. King & Puchnarewicz (2002) proposed that the anti-correlation ($\alpha \sim -4$) is possibly resulted in due to the strong beamed emission in ULXs. Interestingly, the detection of coherent QPO features in BH-ULXs (Atapin et al. 2019; Majumder et al. 2023) indicates the presence of axisymmetric geometrically thin accretion disc, which contradicts the presence of strong beaming (Matteo & Psaltis 1999; Strohmayer & Mushotzky 2003). Furthermore, Middleton et al. (2019) reported that the Lense-Thirring precession of the inner accretion flow can attribute to the origin of the QPOs in ULXs. Meanwhile, Das et al. (2021) argued that the aperiodic modulation of the inner hot 'Comptonizing corona' successfully explains QPO features of BH-ULXs. All these findings clearly indicate the need for an alternative model prescription of accretion dynamics to explain the negative α values in the presence of QPO features.

Table 3. Summary of the observed correlation properties between $L_{\rm disc}$ and $T_{\rm col}$ in different spectral states and the predicted inclinations of the BH-ULXs.

Source	Spectral State†	$L_{\rm disc} - T_{\rm col}$ Correlation Exponent (α)	Predicted Inclination
NGC 5204 X−1	HUL	1.4 ± 0.1	Low
IC 342 X−1	HUL	-3.58 ± 0.04	Moderate
NGC 1313 X−1	HUL	-3.58 ± 0.04	Moderate
NGC 55 ULX1	IUL	-6.01 ± 0.25	High
NGC 6946 X−1	SUL	-8.93 ± 0.11	High
NGC 5408 X−1	IUL	-10.31 ± 0.10	High
NGC 4190 ULX1	HUL	–	Low
M82 X−1	–	–	Low
NGC 4395 ULX1	HUL	–	Moderate

HUL: Hard-ultraluminous state, SUL: Soft-ultraluminous state, IUL: Intermediate-ultraluminous state. †See Sutton et al. (2013)

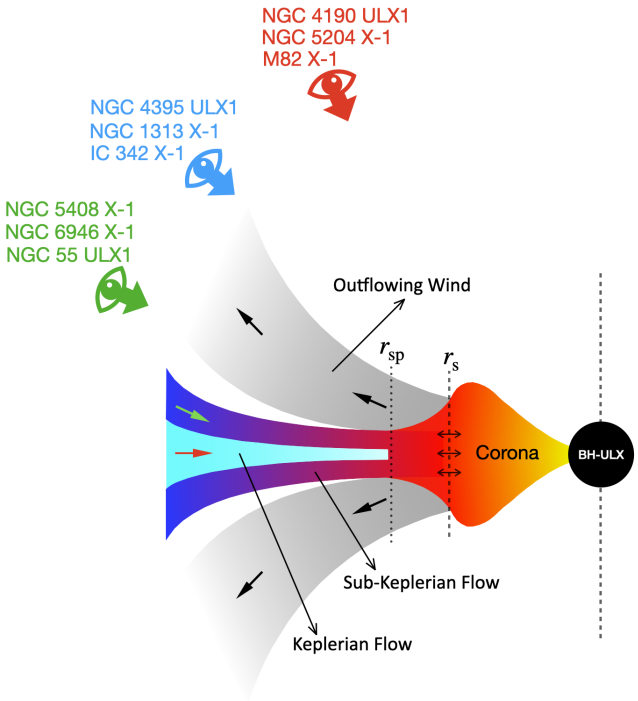

Figure 6. Schematic representation of disc-corona-wind regulated two-component accretion scenario of BH-ULXs. Thick arrows in green, blue and red colors represent the viewing angles of the observer corresponding to high, moderate and low inclinations of sources, respectively. The red, green and black small arrows indicate the direction of the Keplerian flow, sub-Keplerian flow and winds. Here, $r_{\rm s}$ and $r_{\rm sp}$ denote the boundary of the corona and spherization radius. The region $r_{\rm sp} < r < r_{\rm s}$ refers the geometrically thick 'slim disc'. The two-sided black arrows show the radial oscillation of the coronal region around $r_{\rm s}$. See the text for details.

4.4 Alternative Physical Scenario

The limitations of the standard disc and slim disc models in explaining $L_{\rm disc} - T_{\rm col}$ correlations prompt us to explore alternative physically motivated accretion-ejection model prescriptions for BH-ULXs. Such a model prescription appears to be capable in explaining the overall spectro-temporal properties, including $L_{\rm disc} - T_{\rm col}$ correlation and QPO features.

The accretion-ejection model formalism relies on the coexistence of Keplerian and sub-Keplerian flows (Chakrabarti & Titarchuk 1995) and it explains the aspects of spectro-temporal variabilities of BH-XRBs (Chakrabarti & Manickam 2000; Chakrabarti et al. 2009; Debnath et al. 2010; Nandi et al. 2012; Iyer et al. 2015; Sreehari et al. 2019, and references therein). Similarly, this model is expected to explain the spectro-temporal variabilities of BH-ULXs. Further, the non-steady modulation of the Comptonizing corona (with radius $r_{\rm s}$), formed by the sub-Keplerian component, leads to aperiodic variations in the emitted hard X-rays, which may give rise to QPO features (Molteni et al. 1996; Lee et al. 2011; Das et al. 2014; Garain et al. 2014; Debnath et al. 2024). This conjecture effectively explains the mHz QPOs, which have become key observables for constraining the mass, spin, and accretion rate in several BH-ULXs (Das et al. 2021; Majumder et al. 2023). Moreover, by regulating the Keplerian and sub-Keplerian flow components and depending on system inclinations, different spectral states (HUL, SUL, and IUL) can be identified for BH-ULXs (see Table 3). Furthermore, powerful winds are also expected to eject from (a) the boundary of hot coronal region in the inner accretion flow (Chakrabarti 1999; Das et al. 2001; Chattopadhyay & Chakrabarti 2002; Das et al. 2014), (b) standard thin Keplerian disc (Proga et al. 1998; Yang et al. 2018; Raychaudhuri et al. 2021) and (c) super-Eddington (supercritical) slim disc (Poutanen et al. 2007; Dotan & Shaviv 2011), respectively. Moreover, we mention that a model formalism in the framework of relativistic dissipative accretion flow around a rotating black hole has been developed to interpret the luminosity and mHz QPO characteristics of BH-ULXs (Das et al. 2021; Majumder et al. 2023). However, a more comprehensive modeling of the spectral energy distribution to explain the observed spectral characteristics of BH-ULXs is yet to be developed. We depict a schematic representation of the accretion-ejection configuration for the BH-ULXs in Fig. 6.

For super-critical accretion state of BH-ULXs, slim disc model seems relevant, where radiation pressure balances gravity at the spherization radius ($r_{\rm sp}$) resulting in a sub-Keplerian geometrically thick ($H/r \lesssim 1$) disc at $r_{\rm s} \leq r \leq r_{\rm sp}$ (see Fig. 6 and Fabrika et al. 2021). With this, it is apparent that the emission associated with the Keplerian disc ($r > r_{\rm sp}$) is consistent with the standard disc prediction ($L_{\rm disc} \propto T_{\rm col}^4$), whereas the interplay between the inner slim disc and the standard disc at larger radii likely leads to the deviation observed as $L_{\rm disc} \propto T_{\rm col}^{1.4}$ for NGC 5204 X−1. As NGC 4190 ULX1 and NGC 5204 X−1 are observed in the HUL state throughout their long-term spectral evolution (see §4.1), the inner Comptonizing corona, which is the source of non-thermal emission, at $r < r_{\rm s}$ is expected to be visible to the observer, suggesting a low inclination for these two sources (see Fig. 6). In addition, the absence of QPO features in NGC 4190 ULX1 and NGC 5204 X−1 possibly indicates that the radial modulation of the coronal region is either absent or very feeble to be detected. A similar accretion scenario seems to be relevant for M82 X−1 with the exception that oscillation of the corona is prominent enough to produce the observed mHz QPOs (Paper-I, Majumder et al. 2023). Indeed, the prediction of M82 X−1 inclination from the spectral analysis using *XMM-Newton* data could be uncertain because of high contamination. However, it may

be noted that M82 X−1 exhibits coherent mHz QPO features on several occasions that are perhaps associated to the Comptonizing corona (see Majumder et al. 2023). Further, the *Chandra* resolved spectra of the source prefers a slim disc scenario over the standard accretion disc (Brightman et al. 2016). These evidences possibly suggest that M82 X−1 could be a low inclination system, where the inner Comptonizing corona coupled with a slim accretion disc is visible to the observer somewhat similar to the case of NGC 5204 X−1.

In presence of winds, the emitted radiations from the disc interact substantially with the outflowing matter before reaching out to the observer. Due to this, the thermal emission is expected to be cooler with increasing luminosity for super-critical discs in the presence of strong outflowing winds (Poutanen et al. 2007). Considering this, the bolometric luminosity ($L_{\rm bol}$) is estimated as,

$$L_{\rm bol} \approx L_{\rm Edd}\left(1+\frac{3}{5}\ln\dot{m}_0\right); \quad T_{\rm col} \approx 1.5 f_{\rm c} m^{-1/4}\dot{m}_0^{-1/2}, \tag{1}$$

where $T_{\rm col}$ denote the color-corrected temperature at the spherization radius and $\dot{m}_0$ ($= \dot{M}_0/\dot{M}_{\rm Edd} \gg 1$) is the accretion rate. Here, $f_{\rm c}$, $L_{\rm Edd}$, and m are the spectral hardening factor, Eddington luminosity, and mass of the central object scaled in solar mass, respectively. Note that equation (1) leads to an anti-correlation between $L_{\rm bol}$ and $T_{\rm col}$, with a steeper exponent (α) (Poutanen et al. 2007). Furthermore, the outflows from the region $r < r_{\rm sp}$ appear to remain optically thick, and a part of the energy generated within the disc is carried away by the winds. This process expected to reduce the disc temperature and modify the disc luminosity.

The relatively flatter negative correlations ($\alpha \sim -3.58$) observed in the HUL state of IC 342 X−1, NGC 1313 X−1, and NGC 4395 ULX1 suggest an accretion-ejection scenario, where the primary emission is significantly influenced by disc winds. However, the existence of the HUL state indicates that a part of the coronal emission is directly accessible to the observer, suggesting a moderate inclination of the sources (see Fig. 6, Table 3). In contrast, for NGC 55 ULX1, NGC 5408 X−1, and NGC 6946 X−1, the steeper negative correlations ($-10 \lesssim \alpha \lesssim -6$) in the SUL/IUL state likely indicate significant modification of the primary emission due to enhanced winds covering the line of sight. This suggests relatively higher inclinations for these sources (see Fig. 6, Table 3). In both scenarios, it is plausible that the outflowing winds could carry the imprints of oscillations in the Comptonizing region, as predicted by Das et al. (2014), thereby providing a self-consistent explanation for the QPO features observed in IC 342 X−1, NGC 1313 X−1, NGC 5408 X−1, and NGC 6946 X−1. However, the irregular appearance of QPOs throughout the entire *XMM-Newton* monitoring of these sources (see Paper-I, Majumder et al. 2023) suggests that either the necessary resonance condition for modulating the coronal region is not being satisfied, or the oscillation is weak enough to remain undetected.

Moreover, we speculate that the disc-corona-wind symbiosis for two-component super-critical accretion scenario seems to be realistic to explain the spectro-temporal features of BH-ULXs across different spectral states. We also indicate that radiative pressure-driven winds from the super-critical disc possibly govern the correlation between disc luminosity and temperature, and such correlation depends on the source inclination. This conjecture further strengthens the possibility of having a super-Eddington accretion scenario with massive stellar-mass to inter-mediate mass black hole accretors in NGC 5408 X−1, NGC 6946 X−1, IC 342 X−1 and NGC 1313 X−1, as predicted in Majumder et al. (2023).

5 CONCLUSION

In this study, we carry out a comprehensive analysis of the long-term evolution of eight BH-ULXs using *XMM-Newton* observations. Our findings provide compelling evidence for varied accretion scenarios that can explain the observed spectro-temporal variability and (anti-)correlations between disc luminosity ($L_{\rm disc}$) and inner disc temperature ($T_{\rm col}$). The key results from our investigation, along with their potential implications, are summarized below.

- The positive correlation of $L_{\rm disc} \propto T_{\rm col}^{1.4}$ observed for NGC 5204 X−1 suggests a transition from the standard geometrically thin disk ($H/r << 1$) to a slim disk ($H/r \lesssim 1$) prescription at relatively higher luminosities in the HUL state. This behavior is reminiscent of an accretion scenario where both Keplerian and sub-Keplerian flow components coexist.
- A steeper negative correlation with $-10 \lesssim \alpha \lesssim -6$ between $L_{\rm disc}$ and $T_{\rm col}$ is observed for sources NGC 6946 X−1, NGC 55 ULX1, NGC 5408 X−1, which exhibit softer and intermediate spectral characteristics. In contrast, a relatively flatter anti-correlation with $\alpha \sim -3.58$ is seen for IC 342 X−1 and NGC 1313 X−1, which display harder spectral features.
- The diverse $L_{\rm disc} - T_{\rm col}$ correlations along with the overall spectro-temporal characteristics suggest a connection with the disc-corona-wind regulated two-component super-critical accretion scenario. Such scenario also potentially viable to explain the observed QPO features in BH-ULXs. In particular, we infer that the anti-correlations are possibly resulted due to the modification of disc emissions by the outflowing winds, which is also likely to be influenced by moderate to high inclinations of the respective BH-ULXs.

ACKNOWLEDGEMENTS

Authors thank the anonymous reviewer for constructive comments and useful suggestions that help to improve the quality of the manuscript. SM, and SD thank the Department of Physics, IIT Guwahati, for providing the facilities to complete this work. AN thanks GH, SAG; DD, PDMSA, and Director, URSC for encouragement and continuous support to carry out this research. This publication uses the data from the *XMM-Newton* mission, archived at the HEASARC data center. The instrument team is thanked for processing and providing useful data and software for this analysis.

DATA AVAILABILITY

Data used for this publication are currently available at the HEASARC browse website (https://heasarc.gsfc.nasa.gov/db-perl/W3Browse/w3browse.pl).

REFERENCES

Abe Y., Fukazawa Y., Kubota A., Kasama D., Makishima K., 2005, PASJ, 57, 629
Abramowicz M. A., Fragile P. C., 2013, Living Reviews in Relativity, 16, 1
Abramowicz M. A., Czerny B., Lasota J. P., Szuszkiewicz E., 1988, ApJ, 332, 646
Agrawal V. K., Nandi A., 2015, MNRAS, 446, 3926
Alston W. N., et al., 2021, MNRAS, 505, 3722
Aneesha U., Das S., Katoch T. B., Nandi A., 2024, MNRAS, 532, 4486
Arnaud K. A., 1996, in Jacoby G. H., Barnes J., eds, Astronomical Society of the Pacific Conference Series Vol. 101, Astronomical Data Analysis Software and Systems V. p. 17
Atapin K., Fabrika S., Caballero-García M. D., 2019, MNRAS, 486, 2766
Athulya M. P., Radhika D., Agrawal V. K., Ravishankar B. T., Naik S., Mandal S., Nandi A., 2022, MNRAS, 510, 3019
Baby B. E., Bhuvana G. R., Radhika D., Katoch T., Mandal S., Nandi A., 2021, MNRAS, 508, 2447
Bachetti M., et al., 2013, ApJ, 778, 163
Bachetti M., et al., 2014, Nature, 514, 202
Barra F., et al., 2022, MNRAS, 516, 3972
Belloni T., Homan J., Casella P., van der Klis M., Nespoli E., Lewin W. H. G., Miller J. M., Méndez M., 2005, A&A, 440, 207
Belloni T. M., Sanna A., Méndez M., 2012, MNRAS, 426, 1701
Beloborodov A. M., 1998, MNRAS, 297, 739
Bhuvana G. R., Radhika D., Agrawal V. K., Mandal S., Nandi A., 2021, MNRAS, 501, 5457
Brightman M., et al., 2016, ApJ, 829, 28
Caballero-García M. D., Belloni T., Zampieri L., 2013, MNRAS, 436, 3262
Carpano S., Haberl F., Maitra C., Vasilopoulos G., 2018, MNRAS, 476, L45
Chakrabarti S. K., 1995, arXiv e-prints, pp astro–ph/9502040
Chakrabarti S. K., 1999, A&A, 351, 185
Chakrabarti S. K., Manickam S. G., 2000, ApJ, 531, L41
Chakrabarti S., Titarchuk L. G., 1995, ApJ, 455, 623
Chakrabarti S. K., Dutta B. G., Pal P. S., 2009, MNRAS, 394, 1463
Chattopadhyay I., Chakrabarti S. K., 2002, Journal of Astrophysics and Astronomy, 23, 149
Colbert E. J. M., Mushotzky R. F., 1999, ApJ, 519, 89
Das S., Chattopadhyay I., Nandi A., Chakrabarti S. K., 2001, A&A, 379, 683
Das S., Chattopadhyay I., Nandi A., Molteni D., 2014, MNRAS, 442, 251
Das S., Nandi A., Agrawal V. K., Dihingia I. K., Majumder S., 2021, MNRAS, 507, 2777
Davis S. W., El-Abd S., 2019, The Astrophysical Journal, 874, 23
Debnath D., Chakrabarti S. K., Nandi A., 2010, A&A, 520, A98
Debnath S., Chattopadhyay I., Joshi R. K., 2024, MNRAS, 528, 3964
Dewangan G. C., Titarchuk L., Griffiths R. E., 2006, ApJ, 637, L21
Done C., Davis S. W., 2008, ApJ, 683, 389
Dotan C., Shaviv N. J., 2011, MNRAS, 413, 1623
Earnshaw H. M., Roberts T. P., 2017, MNRAS, 467, 2690
Earnshaw H. P., et al., 2019, ApJ, 881, 38
Earnshaw H. P., et al., 2024, The Astrophysical Journal, 968, 111
Fabbiano G., 1989, ARA&A, 27, 87
Fabrika S. N., Atapin K. E., Vinokurov A. S., Sholukhova O. N., 2021, Astrophysical Bulletin, 76, 6
Feng H., Kaaret P., 2009, ApJ, 696, 1712
Feng H., Soria R., 2011, New A Rev., 55, 166
Feng H., Rao F., Kaaret P., 2010, ApJ, 710, L137
Frank J., King A., Raine D. J., 2002, Accretion Power in Astrophysics: Third Edition
Fürst F., et al., 2016, ApJ, 831, L14
Garain S. K., Ghosh H., Chakrabarti S. K., 2014, MNRAS, 437, 1329
Ghosh T., Rana V., 2021, MNRAS, 504, 974
Ghosh T., Rana V., 2023, ApJ, 949, 78
Ghosh T., Rana V., Bachetti M., 2022, arXiv e-prints, p. arXiv:2202.01432
Gierliński M., Done C., 2004, MNRAS, 347, 885
Gladstone J. C., Roberts T. P., Done C., 2009, MNRAS, 397, 1836
Grisé F., Kaaret P., Corbel S., Cseh D., Feng H., 2013, MNRAS, 433, 1023
Gúrpide A., Godet O., Koliopanos F., Webb N., Olive J. F., 2021, A&A, 649, A104
Heil L. M., Vaughan S., Roberts T. P., 2009, MNRAS, 397, 1061
Israel G. L., et al., 2017, Science, 355, 817
Iyer N., Nandi A., Mandal S., 2015, The Astrophysical Journal, 807, 108
Jithesh V., 2022, MNRAS, 509, 5166
Kaaret P., Feng H., 2009, ApJ, 702, 1679
Kaaret P., Feng H., Roberts T. P., 2017, ARA&A, 55, 303
Kajava J. J. E., Poutanen J., 2009, MNRAS, 398, 1450
King A. R., Puchnarewicz E. M., 2002, MNRAS, 336, 445
King A., Lasota J.-P., Middleton M., 2023, New A Rev., 96, 101672
Kosec P., Pinto C., Fabian A. C., Walton D. J., 2018, MNRAS, 473, 5680
Kubota A., Makishima K., 2004, ApJ, 601, 428
Lee S.-J., Ryu D., Chattopadhyay I., 2011, The Astrophysical Journal, 728, 142
Majumder S., Sreehari H., Aftab N., Katoch T., Das S., Nandi A., 2022, MNRAS, 512, 2508
Majumder S., Das S., Agrawal V. K., Nandi A., 2023, MNRAS, 526, 2086
Makishima K., Maejima Y., Mitsuda K., Bradt H. V., Remillard R. A., Tuohy I. R., Hoshi R., Nakagawa M., 1986, ApJ, 308, 635
Makishima K., et al., 2000a, ApJ, 535, 632
Makishima K., et al., 2000b, ApJ, 535, 632
Matteo T. D., Psaltis D., 1999, The Astrophysical Journal, 526, L101
Middleton M. J., Heil L., Pintore F., Walton D. J., Roberts T. P., 2015, MNRAS, 447, 3243
Middleton M. J., Fragile P. C., Ingram A., Roberts T. P., 2019, MNRAS, 489, 282
Miller J. M., Fabbiano G., Miller M. C., Fabian A. C., 2003, ApJ, 585, L37
Molteni D., Sponholz H., Chakrabarti S. K., 1996, ApJ, 457, 805
Mukherjee E. S., et al., 2015, The Astrophysical Journal, 808, 64
Nandi A., Debnath D., Mandal S., Chakrabarti S. K., 2012, A&A, 542, A56
Pasham D. R., Cenko S. B., Zoghbi A., Mushotzky R. F., Miller J., Tombesi F., 2015, ApJ, 811, L11
Poutanen J., Lipunova G., Fabrika S., Butkevich A. G., Abolmasov P., 2007, MNRAS, 377, 1187
Proga D., Stone J. M., Drew J. E., 1998, MNRAS, 295, 595
Quintin E., Webb N. A., Gúrpide A., Bachetti M., Fürst F., 2021, MNRAS, 503, 5485
Rana V., et al., 2015, ApJ, 799, 121
Rao F., Feng H., Kaaret P., 2010, ApJ, 722, 620
Raychaudhuri S., Vyas M. K., Chattopadhyay I., 2021, MNRAS, 501, 4850
Remillard R. A., McClintock J. E., 2006, ARA&A, 44, 49
Rodríguez Castillo G. A., et al., 2020, ApJ, 895, 60
Rybicki G. B., Lightman A. P., 1979, Radiative processes in astrophysics

Sathyaprakash R., et al., 2019, MNRAS, 488, L35
Shakura N. I., Sunyaev R. A., 1973, A&A, 500, 33
Soria R., Ghosh K. K., 2009, ApJ, 696, 287
Sreehari H., Ravishankar B. T., Iyer N., Agrawal V. K., Katoch T. B., Mandal S., Nandi A., 2019, MNRAS, 487, 928
Strohmayer T. E., Mushotzky R. F., 2003, ApJ, 586, L61
Strohmayer T. E., Mushotzky R. F., Winter L., Soria R., Uttley P., Cropper M., 2007, ApJ, 660, 580
Sutton A. D., Roberts T. P., Middleton M. J., 2013, MNRAS, 435, 1758
Vaughan S., Edelson R., Warwick R. S., Uttley P., 2003, MNRAS, 345, 1271
Vierdayanti K., Mineshige S., Ueda Y., 2010, PASJ, 62, 239
Walton D. J., et al., 2013, ApJ, 779, 148
Walton D. J., et al., 2014, ApJ, 793, 21
Walton D. J., et al., 2015, ApJ, 799, 122
Watarai K.-y., Mizuno T., Mineshige S., 2001, ApJ, 549, L77
Wilms J., Allen A., McCray R., 2000, ApJ, 542, 914
Winter L. M., Mushotzky R. F., Reynolds C. S., 2006, ApJ, 649, 730
Xu Y., et al., 2019, ApJ, 879, 93
Yang X.-H., Bu D.-F., Li Q.-X., 2018, The Astrophysical Journal, 867, 100
Yoshida T., Ebisawa K., Matsushita K., Tsujimoto M., Kawaguchi T., 2010, ApJ, 722, 760
Zdziarski A. A., Johnson W. N., Magdziarz P., 1996, MNRAS, 283, 193